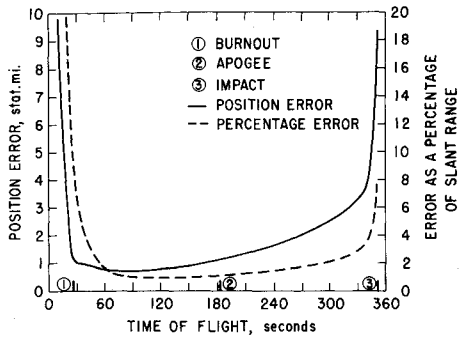

Fig. 3 Accuracy of the trajectory model.

altitude h_b and time t_b are assumed constant with respect to QE and are taken from the original trajectory simulations. Thus $g = 2(H - h_b)/(T - t_b)$.[2] Finally, burnout range, which cannot be assumed constant with respect to QE, is found from a simple linear approximation. If r_{b1} is the range given by the trajectory simulation for QE_1, the burnout range for any other QE is found from $r_b = r_{b1}\,(90° - QE)/(90° - QE_1)$. The coefficients of Eqs. (4–6) may then be evaluated as $y_0 = x_a - 0.5gT^2$, $v_x = gT$, $v_z = (z_a - r_b)/(T - t_b)$, and $z_0 = r_b - v_z t_b$.

Equations (4–6) allow explicit determination of payload position in space at any time, for any given launch QE, AZ, and time. Although of simple form, they accurately represent the trajectory because of their faithfulness to the actual physical situation. The equations yield a trajectory symmetric about the radius vector to apogee, a trajectory that goes through the predicted apogee point at the predicted time, and one that goes through the burnout point at the proper time.

Figure 3 indicates the accuracy of the trajectory model. Two complete trajectory simulations were run for QEs of 80° and 84°, at an azimuth of 140°, for the Nike Iroquois rocket from one particular launch site. The data from these two simulations were used to evaluate the constants of Eqs. (1–3). Then, using the trajectory model described here, position vs time was calculated for a QE of 76° at an AZ of 180°. A third complete trajectory simulation was then run for the same QE and AZ, and position data was compared. The position error plotted in Fig. 3 was calculated as the magnitude of the vector difference between the instantaneous position vectors as gained from the trajectory model and the trajectory simulation. Thus, the position error plotted is the total error and not merely a component of the error.

To calculate position in the trajectory model, azimuth of the trajectory plane XZ was assumed to be $AZ = 180° + \Delta AZ$; where ΔAZ was the change in azimuth of the rocket between launch and apogee as revealed by the trajectory simulation for QE_1. This correction is sufficient so long as a central value of azimuth is used in the trajectory simulation.

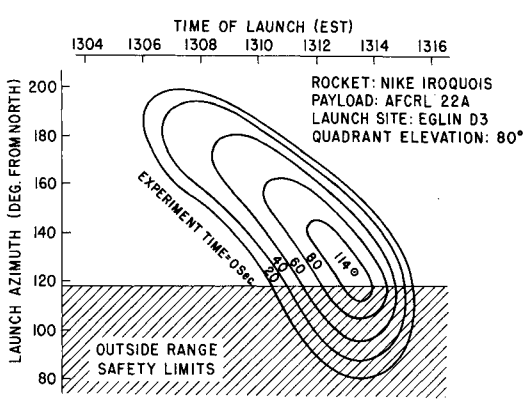

Fig. 4 Time spent in eclipse umbra (experiment time).

Application To Eclipse

Conventional Besselian Elements,[3] with numerical values taken from Ref. 4, were used to specify the eclipse conditions. Details of computations and coordinate systems are given elsewhere,[5] but Fig. 4 is presented as an example of the application of the method to one eclipse payload. Examination of a very large number of trajectories yielded the family of curves shown in less than a minute of computer execution time. In comparison, generating the same curves with repetitive trajectory simulations would have required hours.

References

[1] Schaechter, W., "Sounding Rocket Performance Approximations," *Unguided Rocket Ballistics Meteorology Conference*, Atmospheric Sciences Lab., White Sands Missile Range, N. Mex., 1967, pp. 133–152.

[2] Greenwood, D. T., *Principles Of Dynamics*, Prentice-Hall, N.J., 1965, pp. 65–70.

[3] *Explanatory Supplement To The Astronomical Ephemeris And The American Ephemeris And Nautical Almanac*, Nautical Almanac Offices of the U.K. and the U.S.A., London, 1961, pp. 211–222.

[4] *American Ephemeris and Nautical Almanac for 1970*, U.S. Government Printing Office, Washington, D.C., pp. 294–296.

[5] Herzberg, A. F., "Trajectory Modeling For Efficient Computation Of Rocket/Moving Target Spatial Relationships," AIAA Paper 70-1374, Williamsburg, Va., 1970.

Comparison of Hypersonic Aerodynamic Deceleration Systems Based on Gun-Tunnel Investigation

WOLFGANG WYBORNY* AND HANS-PETER KABELITZ*
Deutsche Forschungs- und Versuchsanstalt für Luft- und Raumfahrt E. V., Porz-Wahn, Germany

Nomenclature

A_F, A_P	=	free and projected area of slotted flares, mm²
C_D, C_L	=	drag and lift coefficients
D	=	diameter of the cylinder, mm
H_s	=	spoiler height, mm
l, l_c	=	lengths of spike and body cylinder, mm
l_s	=	distance of the spoiler from the nose, mm
l_{sep}	=	length of the separated boundary layer, mm
M_∞	=	freestream Mach number
p_t	=	stagnation pressure, atm
$Re_D, Re_{x_{sep}}$	=	Reynolds number based on D and x_{sep}, respectively
T_t	=	stagnation temperature, °K
x_f, x_{sep}	=	distances between nose and junction of flare, and between nose and separation point, mm
β, θ_f	=	spike deflection and flare angles, deg
δ	=	measure of tangential extension of the spoiler, deg
$\vartheta_{sep}, \vartheta_{sh}$	=	separation angle and induced shock angle, deg

Introduction

THIS Note presents results of experimental investigations on aerodynamic deceleration devices for bodies composed of cylindrical main sections and various front sections, i.e.,

Presented as Paper 70-1174 at the AIAA Aerodynamic Deceleration Systems Conference, Dayton, Ohio, September 14–16, 1970; submitted November 6, 1970; revision received April 21, 1971.

* Research Scientist. Member AIAA.

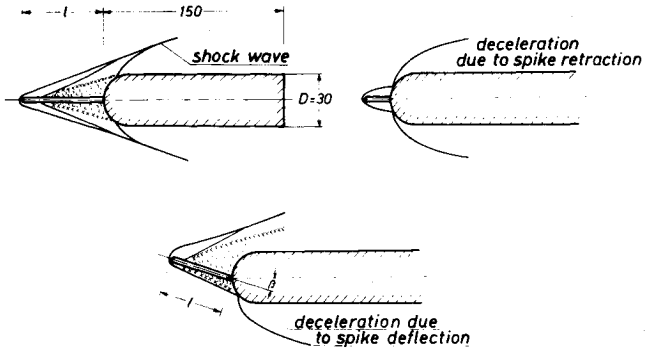

Fig. 1 Concepts for deceleration due to spike retraction or deflection.

hemispheres, cones, and ogives. The deceleration devices were nose spikes, spoilers, and conical slotted or unslotted aft flares. The tests were carried out in a gun tunnel.[1] The test section had a diameter of 22 cm; the testing time was 30 msec. The freestream conditions were: $M_\infty = 8.75$, $T_t = 980°K$, and $p_t = 155$ atm; Re_D was 0.23×10^6 for all investigations. The measurement techniques included Schlieren observations, 3-component force measurements using a fast-response balance,[2] and surface pressure measurements using strain-gage pressure transducers.[3]

Nose Spikes

Nose spikes have been investigated by many authors (e.g., Refs. 4–6). This Note summarizes results[7,8] with respect to aerodynamic deceleration, using the concepts illustrated in Fig. 1. For normal flight conditions, the boundary layer separates at the spike and reattaches at the nose of the body. The aerodynamic effect is that of a conical nose. The drag therefore decreases. If the spike is partially or fully retracted, the drag of the vehicle increases. If the spike is deflected, the flowfield is altered as if a cone were asymmetrically attached to the nose, and a lift force is generated.

Figure 2 shows results for nondeflected spikes for three nose shapes. (The spike nose was hemispherical in all cases.) For the three nose shapes the minimum C_D's are of the same order of magnitude. In the sense of the cone analogy described above, this means that the minimum cone angle is nearly independent of nose shape.

For the conical-nosed model, C_D passes through a maximum at $l/D \simeq 0.5$. For the flat-nosed body unsteady flow regimes were detected by Schlieren observations.[4,6,8]

Figure 3 shows C_D vs spike deflection angle β for the spherical-nosed cylinder. Other nose shapes of the basic model show a similar behavior. Short spikes generate no noticeable drag increase if the spike is deflected. The lift has a maximum at low β's for longer spikes. For higher β's a large drag may be combined with a small lift. Thus, short deflected spikes could be suitable for hypersonic guidance and control,[8] and long spikes for deceleration.

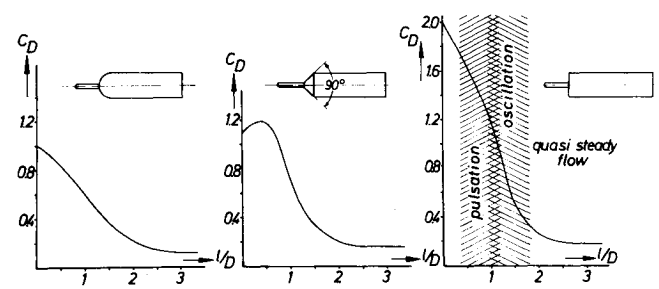

Fig. 2 Measured C_D's vs spike length/body diameter; $M_\infty = 8.75$, $Re_D = 0.23 \times 10^6$.

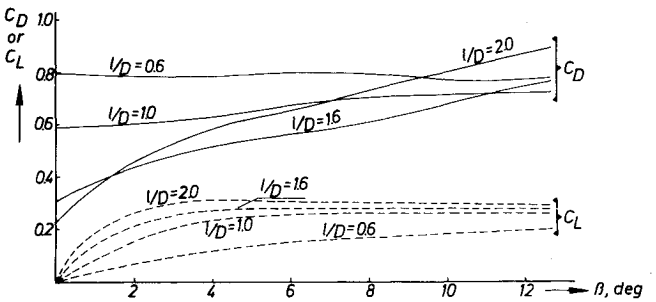

Fig. 3 Drag coefficients for deflected spikes.

Spoilers

Several authors have investigated fixed spoilers in the supersonic region.[9–11] For hypersonic Mach numbers the increases in drag and lift are not as great; an effective increase in drag is obtained only if the spoiler is attached to the nose regime of the basic model in such a way that the nose shock of the basic model is essentially deformed (see Schlieren pictures of Fig. 4). The measured drag coefficients vs tangential spoiler extension (angle δ) are shown in the same figure. For a very high spoiler ($H_s = D/2$) attached near the body nose a significant drag increase is observed. For a smaller spoiler height ($H_s = D/3$) the bow shock of the model is not strongly deformed and there is no significant drag increase. The same results were obtained for two other model types, with spherical and conical noses.[11] No effect on drag could be measured if spoilers were attached to the body further downstream than $l_s/D > 4$, even for very high spoilers ($H_s = D/2$). The maximum tangential extension of a spoiler that was investigated was $\delta = 180°$. An empirical estimation shows no agreement with the measured drag. The reason for this lack of agreement may be seen in the three-dimensional character of the separation region. Because of crossflows the extent of the reversed flow region in front of the spoiler is decreased as shown in the Schlieren pictures. The separation point moves upstream and the reattachment point moves nearer to the outer edge of the spoiler at the line of symmetry if the tangential extension of the spoiler increases. The attempt to obtain empirical relations between tangential spoiler extension and separation angle by means of Schlieren observations was

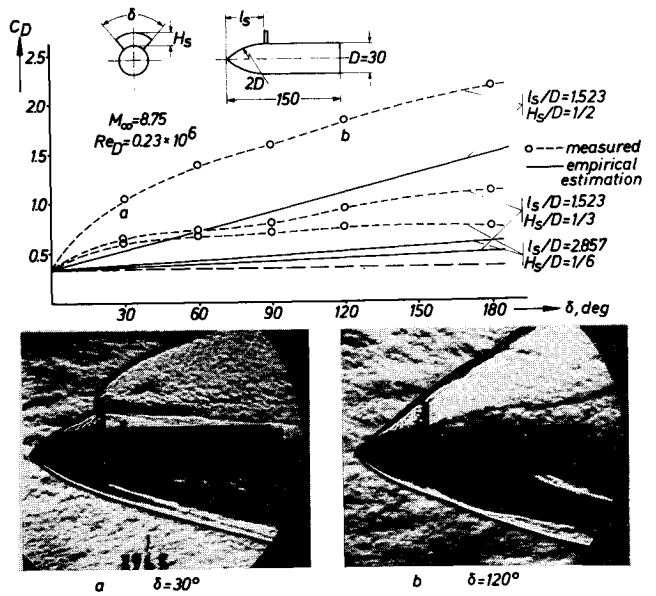

Fig. 4 Results for spoilers of different circumferential extension.

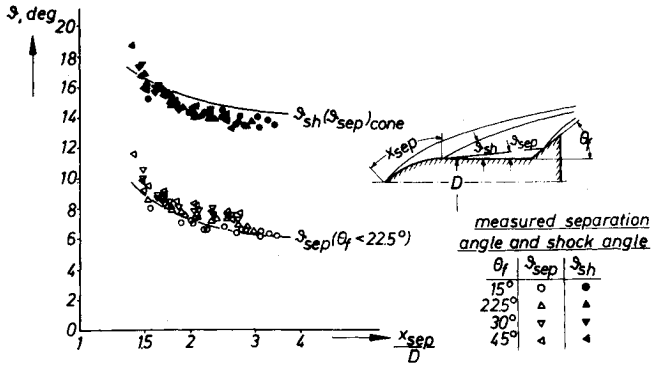

Fig. 5 Separation angle and shock angle vs distance to the separation point.

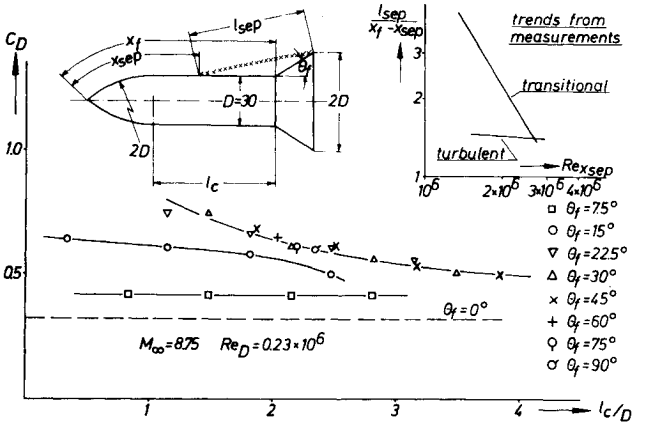

Fig. 7 Drag coefficient vs forebody length for ogive-nosed cylinders with flares.

not successful because of the unsteady behavior of the separated boundary layer.

Flares

For small aft flare angles, the boundary layer remains attached, inducing a conical shock, but for higher flare angles ($\theta_f \geq 15°$) boundary-layer separation occurs. For even higher flare angles the separated boundary-layer reattaches at the outer edge of the flare.[12,13] Figure 5 shows separation angles ϑ_{sep} and induced shock angles ϑ_{sh} on an ogive nosed cylinder obtained from Schlieren pictures. These angles are correlated by the nondimensional distance to the separation point, x_{sep}/D.

High-speed motion pictures show that the separation region becomes increasingly unsteady for $\theta_f > 22.5°$. For $\theta_f < 22.5°$, a good correlation of measured separation and shock angles, and hence the plateau pressure in the separated region, may be obtained by a tangent cone analysis for calculating ϑ_{sh}. The increase in drag may be estimated under the following assumptions[13]: 1) the separated region is axisymmetric; 2) the pressure in the separated region is constant; 3) the cone pressure may be calculated by the Newtonian approximation from local flow values at x_{sep}; and 4) the local flow conditions are calculated from body nose shape and local surface pressure measurements on a model with no separation. Figure 6 shows the drag obtained by an empirical method compared with the measurements for conical flared models with spherical and ogive noses. The agreement seems to be satisfactory even for larger flare angles where the separated boundary layer showed an unsteady behavior. Both configurations show a maximum for $\theta_f \simeq 45°$ when, in each case, total model length remains constant and the base diameter of the flares is twice the diameter of the cylindrical model. For comparison, Fig. 6 shows the results of similar calculations for the case with no boundary-layer separation. In the first example the pressure coefficient is based on freestream conditions and in the second on local flow conditions at the point where the flare is fitted to the main body. This comparison shows the important influence of boundary-layer separation on the deceleration effectiveness of a flared body.

Figure 7 shows that there is no measurable influence of forebody length on drag if the flare angle is $\theta_f = 7.5°$, because no boundary-layer separation occurs. For $\theta_f \geq 15°$, the drag decreases with increasing forebody length. For $\theta_f \geq 22.5°$, all measured points are fitted by one curve, i.e., for fixed values of l_c and flare base diameter, drag is independent of θ_f and remains constant. This may be explained by the behavior of the separated boundary layer as follows: the parameter $l_{sep}/(x_f - x_{sep})$ shows for $\theta_f = 15°$ a strong dependence on the local Reynolds number (Fig. 7, sketch at upper right). Higher flare angles show a weaker dependence.

The deceleration effectiveness of conical flares is reduced because of boundary-layer separation. Also, boundary-layer separation may be prevented or at least significantly reduced by suction or by cross flows which may be established by slotting the flares.[14] The slotted flares consist of six elements with a lateral extension h. Their length is given by the base diameter, which again is $2D$. As before (Fig. 6), the total model length is constant. Figure 8 shows C_D vs the so-called "free area ratio" A_F/A_P of the slotted flare for ogive-nosed models with different flare angles. For all angles the drag may be increased by slotting the flares. For increasing flare angles the drag maximum is shifted toward higher "free area ratios" A_F/A_P. The deceleration efficiency of slotted flares

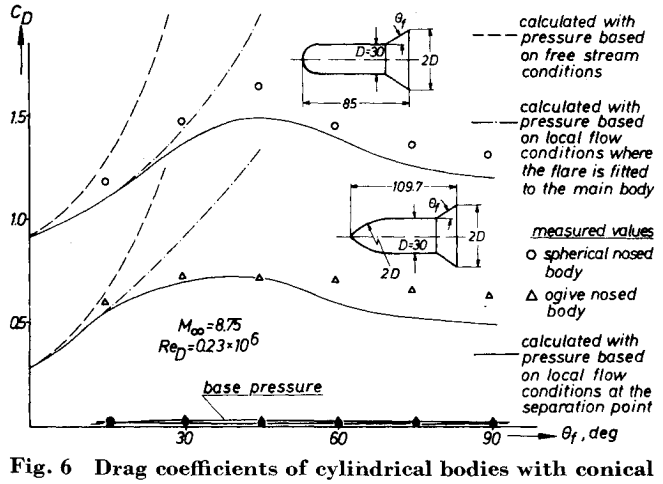

Fig. 6 Drag coefficients of cylindrical bodies with conical flares vs flare angle.

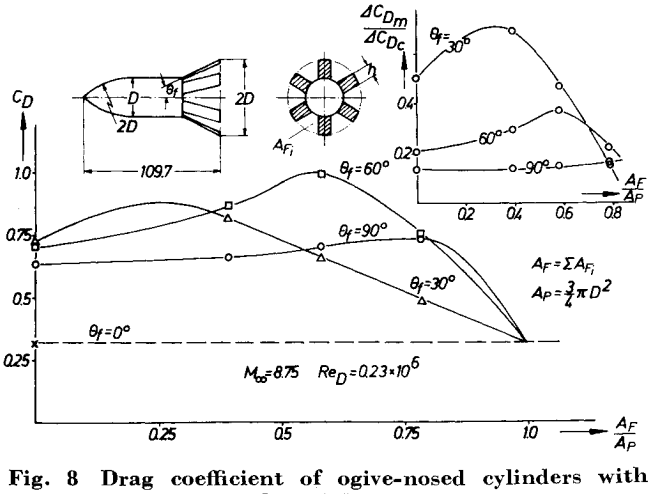

Fig. 8 Drag coefficient of ogive-nosed cylinders with slotted flares.

may be defined from the ratio of the measured increase in drag for a slotted flare to the calculated increase in drag for an unslotted non-separating flare ($\Delta C_{D_m}/\Delta C_{D_c}$).

Conclusions

Conical slotted or unslotted flares create drag without lift. Models with fixed spoilers show a strong coupling between lift and drag. Cylindrical bodies with spikes permit a wide variation of drag and independent variation or adjustment of lift forces if changes in spike length and spike deflection angles are considered.

References

[1] Wyborny, W. and Kabelitz, H.-P., "Funktionsuntersuchungen und erste Versuchsergebnisse im Stoßwellenwindkanal mit freifliegendem Kolben," DLR FB 65-43, July 1965, Deutsche Versuchsanstalt für Luft- und Raumfahrt, Porz-Wahn, Germany.

[2] Heyser, A., Wyborny, W., and Kabelitz, H.-P., "Dreikomponentenmessungen an den AGARD-Eichmodellen HB-1 und HB-2 in Stoßwellenwindkanal mit freifliegendem Kllben," DLR FB 66-25, April 1966, Deutsche Versuchsanstalt für Luft- und Raumfahrt, Porz-Wahn, Germany.

[3] Kabelitz, H.-P., Weber, P.-J., and Wyborny, W., "Entwicklung eines Druckgebers kurzer Ansprechzeit auf der Basis von Dehnmeßdrähten für Messungen bei geringen Dichten," DLR FB 68-53, Aug.1968, Deutsche Versuchsanstalt für Luft- und Raumfahrt, Porz-Wahn, Germany.

[4] Wood, C. J., "Hypersonic Flow Over Spiked Cones," *Journal of Fluid Mechanics*, Vol. 12, 1962, pp. 614–624.

[5] Thurman, W. E., "A Flow-Separation Spike for Hypersonic Control of a Hemisphere-Cylinder," *AIAA Journal*, Vol. 2, No. 1, Jan. 1964, pp. 159–161.

[6] Holden, M. S., "Experimental Studies of Separated Flows at Hypersonic Speeds, Part I: Separated Flows Over Axisymmetric Spiked Bodies," *AIAA Journal*, Vol. 4, No. 4, April 1966, pp. 591–599.

[7] Heyser, A., Wyborny, W., and Kabelitz, H.-P., "Kraftmessungen an stumpfen Körpern im DVL-Stoßwellenwindkanal mit freifliegendem Kolben (M = 8 bis 16)," DLR FB 67-53, Aug. 1967, Deutsche Versuchsanstalt für Luft- und Raumfahrt, Porz-Wahn, Germany.

[8] Wyborny, W., "Der Einfluß eines ausgelenkten Zentralstiftes auf die aerodynamischen Beiwerte rotationssymmetriescher Hyperschallflugkörper," DLR FB 69-37, June 1967, Deutsche Versuchsanstalt für Luft- und Raumfahrt, Porz-Wahn, Germany.

[9] Bogdonoff, S. M. and Keppler, C. E., "Separation of a Supersonic Turbulent Boundary Layer," *Journal of Aeronautical Science*, Vol. 22, No. 6, June 1955, pp. 414–424.

[10] Heyser, A. and Maurer, F., "Experimental Investigations on Solid Spoilers and Jet Spoilers at Mach Numbers of 0.6 to 2.8," J.P.L. Translation 32, Feb. 1964, Jet Propulsion Lab. California Institute of Technology, Pasadena, Calif. Translated from *Zeitschrift für Flugwissenschaften*, Vol. 10, No. 4/5, May 1962.

[11] Wyborny, W. and Kabelitz, H.-P., "Untersuchungen über den Einfluß eines festen Spoilers auf die aerodynamischen Beiwerte rotationssymmetrischer Körper im Hyperschall," DLR Mitt. 69-24, Dec. 1969, Deutsche Forschungs- und Versuchsanstalt für Luft- und Raumfahrt, Porz-Wahn, Germany.

[12] Kabelitz, H.-P. and Wyborny,W., "Das Ablöseverhalten laminarer Grenzschichten an rotationssymmetrischen Modellen mit konischer Heckerweiterung," DLR FB 69-62, Sept. 1969, Deutsche Forschungs-und Versuchsanstalt für Luft- und Raumfahrt, Porz-Wahn, Germany.

[13] Schepers, H.-J., Wyborny, W., and Kabelitz, H.-P., "Der Einfluß einer konischen Heckerweiterung auf die aerodynamischen Beiwerte zylindrischer Körper im Hyperschall," DLR FB 69-69, Sept. 1969, Deutsche Forschungs-und Versuchsanstalt für Luft- und Raumfahrt, Porz-Wahn, Germany.

[14] Kabelitz, H.-P. and Wyborny, W. "Die aerodynamischen Beiwerte zylindrischer Körper mit Heckspreizschirmen," DLR FB 69-94, Dec. 1969, Deutsche Forschungs- und Versuchsanstalt für Luft-und Raumfahrt, Porz-Wahn, Germany.

Astrobee D: An Advanced Technology Meteorological Rocket Vehicle

R. B. Jenkins* and J. P. Taylor†
Space General Company, El Monte, Calif.
and
T. P. Browne‡ and L. A. Briggs§
Aerojet Solid Propulsion Company, Sacramento, Calif.

SPACE General Company, a Division of Aerojet-General Corporation, conducted a study for NASA in 1968 to apply advanced propulsion techniques to small rocket vehicles for low-cost, high-reliability soundings in the near-Earth region 50 km–140 km (D region for physics and synoptic meterological applications). Existing propulsion units capable of operation in this region were deemed to be too large, too expensive or unreliable. Emphasis was placed on the investigation of new propulsion techniques, including self-pressurizing and monopropellant liquids, and long-burning solids.

Ground rules selected for this study on the basis of mission analysis were as follows: a) single stage, dual-thrust propulsion; b) complete vehicle weight, in meteorological configuration, not to exceed 200 lb; c) gross payload weight of 20 lb with a net useful 10 lb for the meteorological configuration; d) fineness ratio (length/diameter propulsion unit) on the order of 15–20; and e) acceleration level not over 25 g's.

In addition, optimization studies conducted at that time indicated performance, stability and dispersion requirements were optimized with a vehicle of approximately 1 sec boost at 4000 lb thrust followed by 20–30 sec of sustain thrust at a lower level.

The motor design parameters given in Table 1 were established after an extensive survey of using agencies. Although they did not meet every requirement of all agencies, they provided substantial improvements over existing systems.

Previous studies have indicated that to acheive a 140-km altitude would require either a boosted-Dart type of vehicle or a two-stage vehicle. Either staging concept reduces the inherent reliability of the system and potentially adds cost by the addition of a second stage, either inert or propulsive.

Table 1 Astrobee D design features

Boost/sustain thrust level ratio	~3:1
Maximum diam., in.	6
Max. length, in.	110
Motor wt, lb	181
Propellant wt, lb	133
Inert wt, lb	45
Duration, sec	15 minimum
Total impulse (vac 70°F) lb-sec	33,000 minimum
Temperature limits, °F	−40 to +135 −65 (goal)
Max. spin rate, rps	10
Lift-off accel. (motor +20 lb) g's	15 minimum
Max. acceleration (motor + 20 lb) g's	20 maximum
Minimum wall thickness	0.046
Performance with 10 lb of structure (include fins, ogive, shroud) ft	10 to 450,000 minimum

Presented as Paper 70-1387 at the AIAA 2nd Sounding Rocket Technology Conference, Williamsburg, Va.; December 7–9, 1970; submitted December 21, 1970; revision received February 26, 1971.

* Manager, Astrobee Vehicles.

† Engineering Specialist, Astrobee Vehicles. Member AIAA.

‡ Manager, Space Motor Programs, Advanced Motor Operations.

§ Manager, Launch Vehicle Motors, Space Motor Programs, Advanced Motor Operations.